Laser and Particle Beams (2017), *35*, 92–99.

doi:10.1017/S026303461600077X

Influence of hot electrons on the spectra of iron plasma irradiated by femtosecond laser pulses with 10^{21} W/cm^2 intensities

A. STAFFORD,[1] A.S. SAFRONOVA,[1] A.Ya. FAENOV,[2,3] T.A. PIKUZ,[3,4] R. KODAMA,[2,4] V.L. KANTSYREV,[1] I. SHRESTHA,[1] AND V.V. SHLYAPTSEVA[1]

[1]Physics Department, University of Nevada, Reno, NV 89557, USA
[2]Institute for Academic Initiatives, Osaka University, Suita, Osaka 565-0871, Japan
[3]Joint Institute for High Temperatures, Russian Academy of Sciences, Moscow 125412, Russia
[4]PPC and Graduate School of Engineering, Osaka University, Suita, Osaka 565-087, Japan

(RECEIVED 11 October 2016; ACCEPTED 12 November 2016)

Abstract

The use of laboratory experiments as plasma creating sources is a valuable tool for understanding astrophysical observations. Recently plasma created through irradiation by lasers with relativistic intensities has been used to study effects of hot electrons and X-ray pumping on X-ray formation of multiply charged ions spectra. This paper discusses the formation of *K*-shell Fe spectra recorded from a plasma irradiated by 35 fs pulses with intensities of 10^{21} W/cm^2. Modeling of the spectra suggests three different regions of plasma radiation including a cold ~10 eV region, a mild ~700 eV region, and a hot ~3500 eV region. The influence of hot electrons and X-ray pumping is discussed and a comparison with *K*-shell Fe spectra from a 1 MA X-pinch experiment is included to highlight the differences due to the shorter time frame of the laser–plasma interaction experiment.

Keywords: Relativistic laser plasma; X-ray sources; X-ray spectroscopy

1. INTRODUCTION

Observations of astrophysical phenomena have been a continual source of X-ray spectra for many years. Through spectroscopic analysis, these spectra provide clues to understanding the processes that create the various plasmas seen throughout the universe. The spectra point out gaps in our understanding, such as important lines and atomic data details, and targeted laboratory experiments can help fill in those gaps (Beiersdorfer, 2003). Iron is an important element in solar (Rajmal *et al.*, 2006; Phillips, 2012) and other star systems (Eze, 2014; Ponti *et al.*, 2015) and for that reason X-ray Fe spectra have been studied in laboratory experiments using many different plasma sources, including: Electron beam ion traps (Decaux *et al.*, 1995, 1997, 1999), tokamaks (Beiersdorfer *et al.*, 1993, 2001), and X-pinches (Safronova *et al.*, 2009).

Iron is the heaviest element that can be created by the fusion process that occurs in stars as the energy created by the fusion becomes greater than the necessary energy to fuse after iron. This can only occur in the largest stars, however, when a star goes supernova it can create iron quickly along with heavier elements due to the high density of energy and neutrons. Additionally due to being the heaviest element with a positive energy of formation, heavier elements are likely to decay to iron over time. The presence of iron in an astrophysical spectrum can provide information on the history of the object.

Short pulse lasers have been a useful tool in studying X-ray radiation (for example, Magunov *et al.*, 2003 and Abdallah *et al.*, 2007). There have been many improvements in the understanding of Fe X-ray spectra, however, there is more to learn about the different processes involved in X-ray formation with respect to the roles of fast electron beams and X-ray pumping for spectra in laboratory and astrophysics for both low and high density plasmas. It has been found that the plasma created by irradiation from a 500 fs pulse laser on solid targets include a hotter region along the surface with the solid material remaining cold (Chen *et al.*, 2009). The radial direction of plasma from irradiation of a 330 fs pulse laser was also explored with spectroscopy (Zastrau

Address correspondence and reprint requests to: A. Stafford, Department of Physics, University of Nevada, (0220) 1664 N. Virginia St. Reno, NV 89557, USA. E-mail: austins@unr.edu

et al., 2010). One of the important points is to understand the possible role of X-ray photo pumping. In recent investigations with ultra-relativistic laser-produced plasma it was found that photo-pumping was affecting the spectra of medium z targets such as Al (Colgan *et al.*, 2013; Pikuz *et al.*, 2013; Hansen *et al.*, 2014; Faenov *et al.*, 2015*a*) and Si (Colgan *et al.*, 2016). It was shown in (Faenov *et al.*, 2015*a*) that femtosecond laser pulses with intensity reaching 10^{21} W/cm^2 at the surface of some microns Al foils could generate X-ray source with intensity of 10^{17} W/cm^2 and such intensity is already enough for photo-pumping generation of hollow KK and KL ions. Understanding KK and KL ions are of value for diagnosing non-ideal plasma and warm dense matter (Colgan *et al.*, 2008; Faenov *et al.*, 2015*b*). Here spectra of higher z material (Fe) collected from the same experimental conditions as seen in the Al experiments are analyzed to see the roles of fast electron beams and X-ray pumping.

2. EXPERIMENT

The experiments are performed using the J-KAREN (Kiriyama *et al.*, 2010; Nishiuchi *et al.*, 2015), an optical parametric chirped-pulse amplification (OPCPA) Ti:Sapphire hybrid laser system at Kansai Photon Science Institute of Japan Atomic Energy Agency. Laser pulses have the energy on the target up to ~7 J, duration of 35 fs (full width at half maximum, FWHM, with respect to intensity), wavelength of 0.8 μm and a typical contrast of 10^{10} (with respect to power; at several picoseconds before the pulse peak). The contrast is improved with a saturable absorber inserted between the high-energy CPA oscillator and stretcher. The ultrafast Pockels cell with the extinction ratio of 200 is applied at 500 ps before the main pulse to secure the contrast on the nanosecond time scale. Using F/2.1 off-axis parabolic mirror, p-polarized laser pulses are focused onto a target at an incidence angle of 84°, producing a spot with the FWHM diameter of ~4.5 μm (FWHM) and the peak laser intensity of 10^{21} W/cm^2.

The targets are 2 μm stainless steel Fe foils placed at the laser focus position with a 5 μm accuracy along the laser-propagation axis, well within the Rayleigh length of 20 μm. For high-resolution spectroscopy measurements (Faenov *et al.*, 2015*a*) a Focusing Spectrometer with Spatial Resolution (FSSR) (Faenov *et al.*, 1994; Blasco *et al.*, 2001) was implemented. The instrument was equipped with a spherically bent quartz (31–40) crystal with a lattice spacing $2d \sim 2.36$ Å and a radius of curvature of $R = 150$ mm. The crystal was aligned to record K-shell emission spectra of multi-charged (He_α line of Fe XXV and Ly_α line of Fe XXVI) and neutral (i.e. K_α, K_β lines) Fe ions in 1.7–1.97 Å wavelength range. The FSSR spectral resolving power was approximately 3000. The spectrometer observed the laser-irradiated front surface of the target at an angle of ~40° to the target surface normal and the target-to-crystal distance of 2045 mm. Background fogging and crystal fluorescence due to intense fast electrons were limited using two pairs of 0.5 T neodymium-iron-boron permanent magnets that formed a slit ~15 mm wide in front of the crystal. Spectra were recorded on X-ray Andor DX-420 back-illuminated charge-coupled device (CCD) with 26 μm pixel size. The X-ray CCD was protected against exposure to visible light using two layers of 1 μm thick polypropylene coated from both sides with 0.2 μm Al. Additionally, polypropylene filter of 6 μm thickness was used to reduce the background noise. Spectra were measured in single laser shots.

The spectra from the J-KAREN experiments are compared with Stainless Steel (69% Fe, 19% Cr, 9% Ni) X-pinch experiments performed on the Zebra Generator at the Nevada Terawatt Facility at the University of Nevada, Reno. The Zebra generator is a pulsed power device capable of storing up to 150 kJ of energy. That energy is released to provide ~1 MA of current with a 100–110 ns rise time (see, for example, Kantsyrev *et al.*, 2006). The X-pinches were composed of four wires crossed in an X pattern with a 31.7° angle between the wires on the anode and cathode sides. The wires were 40 μm thick providing a 415 μg/cm linear mass through a 20 mm anode to cathode gap. X-ray spectra were recorded using a time integrated spatially resolved spectrometer using a LiF crystal ($2d = 4.028$ Å). The spectrometer was capable of recording over a spectral range of 1.5–2.3 Å and used a 8 μm Kapton Polyimide, 0.3 μm Al, and 2 μm Polypropylene filter.

3. THEORETICAL MODELING

The K-shell Fe experimental spectrum from plasmas irradiated by ultra-intense laser beams with femtosecond scale pulse duration is expected to be primarily dominated by three distinct regions. The first is the hottest region. Despite the high 10^{10} laser contrast in our experiments, at laser intensities ~10^{21} W/cm^2 preplasma is still created. This preplasma will be energized prior to the main pulse, which would then arrive and the already excited material would further excite to the hottest region of the experiment. This would be most strongly composed of H-like, He-like, and Li-like Fe. It would be expected to have an electron temperature (T_e) between 3000 and–4000 eV with optimal absorption of the main pulse when the electron density (N_e) is around 2×10^{21} cm^{-3}, which for our case corresponded laser critical intensity.

The second region would be characterized by the portions of solid material that remain after the prepulse that are hit by the main pulse. This would create cooler plasma than the first region due to the higher density of the material. For neutral Fe, the solid density is 8.25×10^{22} atoms/cm^{-3}. This region would be expected to be dominated by ionizations between Li-like and Ne-like Fe with an average ion charge of +22–24, which would suggest N_e for this region should be around 2×10^{24} cm^{-3}.

The third region would be the material that does not directly interact with either the prepulse or main pulse. This

https://doi.org/10.1017/S026303461600077X Published online by Cambridge University Press

region would be heated by the radiation transfer and hot electrons from the previous two regions. This would create relatively cold temperature plasma (10–50 eV) that is likely to be dominated by ionizations near neutral Fe. This plasma would be close to solid density with an average ion charge around +1–3. This suggests N_e should be around 8×10^{22}–2×10^{23} cm^{-3}.

Theoretical spectra were obtained using two models: One for ionic transitions and one for characteristic transitions. The ionic model was previously developed to study stainless steel Z-pinch wire arrays (Safronova *et al.*, 2008, 2009; Ouart *et al.*, 2011). The model is based on atomic data calculated by the Flexible Atomic Code (Gu, 2008). Ground states for ionization levels from bare to neutral were used, while excited states for H-like to Al-like were detailed with the largest focus being on O-like to Al-like states. For *K*-shell transitions, singly excited states up to $n = 6$ were used for H-like ions, $n = 5$ for He- and Li-like ions, and up to $n = 4$ for Be- to F-like. Doubly excited states were included for He- and Li-like ions up to $n = 3$ and for Be-like up to $n = 2$. The model is run assuming nonlocal thermodynamic equilibrium conditions and synthetic spectra are created by broadening line emissions using Voigt line profiles. The characteristic model includes ground states for all ionization levels with excited states focusing on the K- to Fe-like ionization levels. Singly excited states up to $n = 3$ were included for the K- to Fe-like ionization levels.

Figure 1 shows the spectrum recorded from the J-KAREN experiment (Nishiuchi *et al.*, 2015) with modeling. Three models are included that correspond with the expected predicted regions. Figure 1a covers the first expected region. The plasma parameters used to model this region were $T_e = 3500$ eV, $N_e = 3 \times 10^{21}$ cm^{-3}, and 0.1% hot electrons. T_e was determined by matching the relative ratios of the Heα and Lyα (1.78 Å) lines. N_e was determined by matching the relative ratios of the Heα line with the intercombination (I.C.) line (1.86 Å). The hot electron concentration was most noticeable in the intensities of the H-like, He-like, and Li-like transitions. Increasing the hot electron concentration further emphasized the He-like transitions while the reducing the H-like and Li-like transitions.

The modeling in Figure 1b covers the second expected region. The modeling suggest plasma parameters of $T_e =$ 700 eV, $N_e = 1.8 \times 10^{24}$ cm^{-3}, and 0.1% hot electrons. This modeling primarily covers Li-like to C-like transitions. Changes to T_e shift the ionization balance of the plasma. The T_e for this region was determined by adjusting the ionization balance such that Be-like transitions (~1.87 Å) are the most prominent. Increasing N_e broadens the ionization distribution while decreasing N_e narrows the distribution. N_e was determined by matching the relative intensities of the Be-like, B-like and C-like structures. The presence of hot electrons effected the higher ionizations most significantly. Therefore the hot electron concentration was chosen by

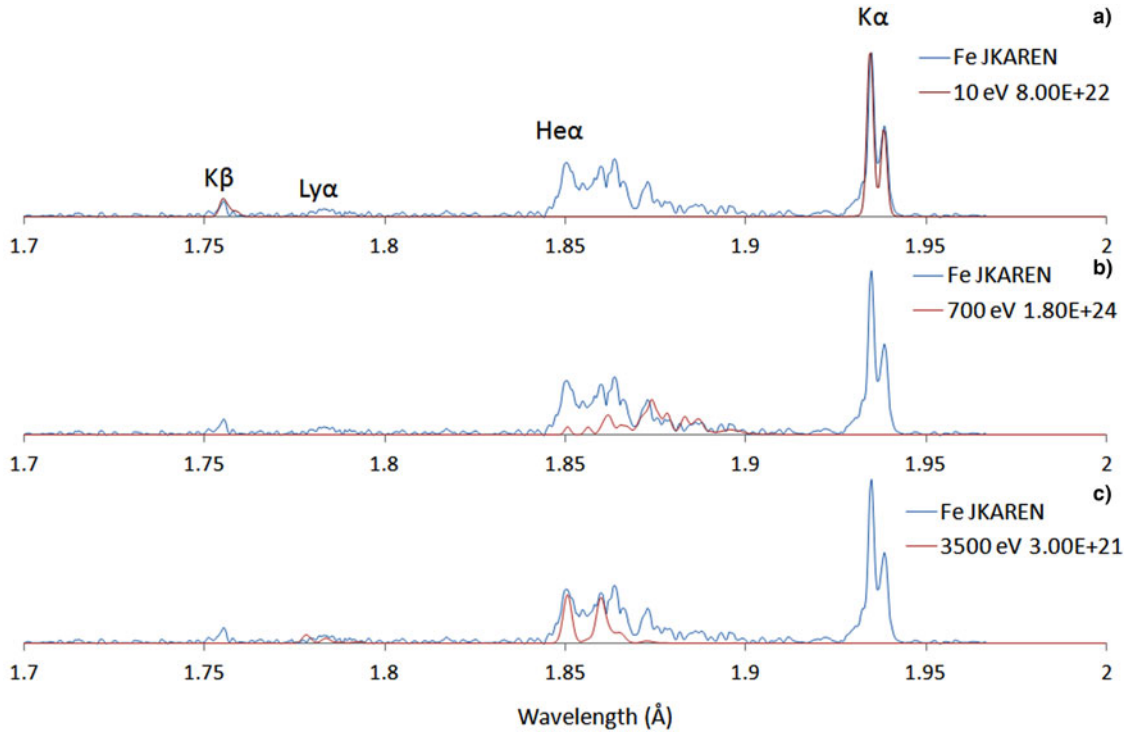

Fig. 1. Theoretical modeling matched to experimental data from laser experiments performed at JKAREN facility (Colgan *et al.*, 2016). All models include 0.1% hot electrons described with a Gaussian distribution at 10 keV with a 50 eV half width at half max (HWHM). (a) 3500 eV and 8×10^{22} cm^{-3} modeling matches Heα and Lyα transitions. (b) 700 eV and 1.8×10^{24} cm^{-3} modeling matches B-like and C-like structures between 1.88 and 1.9 Å. (c) Modeling for cold Kα and Kβ transitions suggest 10 eV electron temperatures with a 8×10^{22} cm^{-3} electron density.

https://doi.org/10.1017/S026303461600077X Published online by Cambridge University Press

looking at the He-like, Li-like, and Be-like contributions to the spectrum.

Figure 1c compares the experimental spectrum with a model with plasma parameters of: $T_e = 10$ eV, $N_e = 8 \times 10^{22}$ cm^{-3}, and 0.1% hot electrons with 10 keV temperature with 50 eV half width at half max. These plasma parameters describe the Kα and Kβ transitions near 1.93 and 1.75 Å, respectively. The T_e was determined by aligning the location of the Kβ lines in the experimental and theoretical spectra. The Kβ transitions shift toward lower wavelengths with increasing T_e quicker than the Kα transitions. The N_e is determined by matching the relative intensities of the two peaks in the Kα region. The Kα peaks are also influenced by the concentration of hot electrons. The presence of hot electrons increases the relative intensity of peak at the longer wavelength. While the presence of hot electrons was a significant change to the modeling, varying the concentration of the hot electrons created very small changes to the modeling. This prevented a precise determination of the hot electron concentration in this region. A 0.1% concentration was used for the modeling as it was found to be a good match for the other regions in which the hot electron concentration is more noticeable.

Figure 2 compares the combined theoretical spectra from Figure 1 with the experimental spectra. The combined spectrum shows good comparison with the cold Kα and Kβ regions and with the Be-like, B-like, and C-like transitions. The most noticeable differences are surrounding the I.C. line. This is possibly due to some differences in wavelengths between the theoretical calculations and the experimental spectrum. The theoretical line for the Li-like peak just to the right of the I.C. line is closer to the I.C. line leading to more of a build up instead of a split peak. Also the theoretical line for the peak between the Heα and I.C. line is shifted close to the I.C. line. This leads to the peak getting absorbed into the I.C. line when trying to broaden the He-like transitions rather than rising to fill the region.

Figure 3 is a comparison of the experimental spectrum with three models that include a very high concentration of hot electrons in a mild T_e (300 eV) bulk plasma with the intent to describe the hotter plasma using one plasma region. The three concentrations are (a) 10%, (b) 25%, and (c) 40%, which were chosen to display the effects of hot electrons on the theoretical spectrum. The 40% is beyond any expectations of what would exist physically but it is useful for highlighting the effects of hot electrons. Figure 3a displays the 10% hot electron concentration and it covers the lower ionization states without any significant presence of the He- and Li-like ions. Figure 3b is the 25% hot electron concentration and it has a balance between the higher (He- and Li-like) and the lower (B- and C-like) ionization levels. This balance does not fit with the experimental spectrum as the higher ionizations are underrepresented and the lower ionizations are slightly overestimated. Figure 3c is the 40% concentration and it matches the higher ionizations closer while the lower ionizations are underestimated. This figure confirms that the hotter plasma cannot be a single region of mild T_e with a high hot electron concentration.

Figure 4 displays a *K*-shell Fe experimental spectrum recorded during a stainless steel X-pinch experiment performed on the Zebra generator at 1 MA. Three theoretical spectra are compared with the experimental spectrum to point out the differences of the X-pinch spectrum and the laser-produced spectrum. The theoretical spectra were modeled at $T_e = 170$ eV and $N_e = 1 \times 10^{20}$ cm^{-3} with varying hot electron concentrations (1, 2.5, and 4%). The laser-produced spectrum was dominated by fewer regions that were relatively easy to distinguish, while the X-pinch spectrum is composed of significant contributions from all the ionizations between He-like and Ne-like Fe, which occurs as the plasma ionizes throughout the experiment.

Figure 5 is the experimental spectrum for the X-pinch compared with two theoretical spectra that describe the maximum and minimum temperature regions represented in the experimental spectrum. The cold region is estimated with $T_e = 170$ eV and $N_e = 1 \times 10^{20}$ cm^{-3}. This is primarily Ne-like transitions that fill in the largest peak in the spectrum. T_e is estimated by matching the location of the Kα peak with the theoretical spectrum. N_e is chosen by using the value from the hot region as the density cannot be properly estimated using one line. The hottest region is estimated

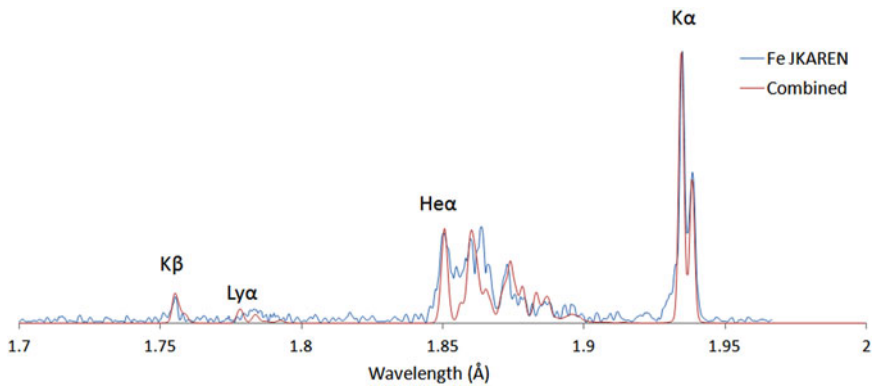

Fig. 2. Combination of theoretical models shown in Figure 1 matched to the experimental spectrum. The modeling matches most structure between 1.85 and 1.95 Å.

https://doi.org/10.1017/S026303461600077X Published online by Cambridge University Press

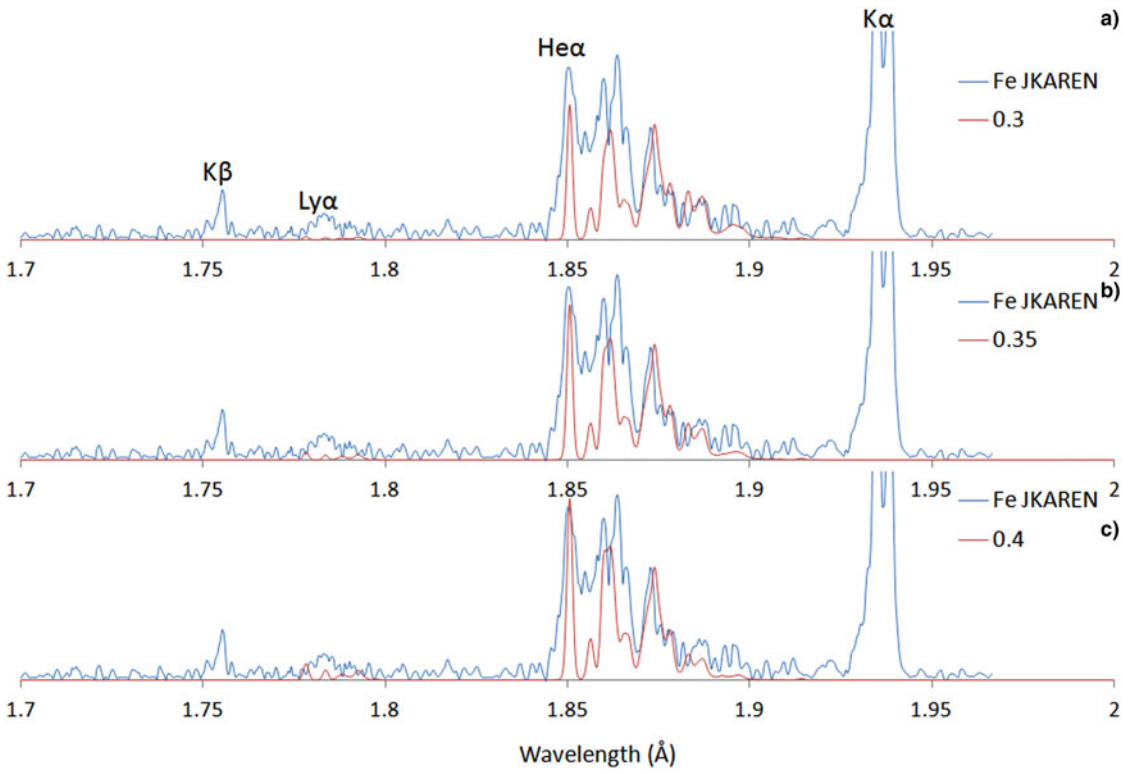

Fig. 3. Theoretical modeling of three different hot electron concentrations, (a) 10%, (b) 25%, and (c) 40%, with a bulk $T_e = 300$ eV and $N_e = 1.8 \times 10^{24}$ cm^{-3}. The modeling shows the ionization balance does not fit the experimental spectrum which confirms the need for multiple regions shown in Figure 1.

with $T_e = 1700$ eV and $N_e = 1 \times 10^{20}$ cm^{-3}. N_e is estimated by matching the relative intensities of the Heα line with the I.C. line. T_e is estimated with less accuracy as there is not a Lyα line presence with which to compare the Heα line.

4. DISCUSSION

The laser-produced spectrum was describable with the three predicted plasma regions: (1) The preplasma region irradiated by both the prepulse and the main pulse, (2) the solid density plasma from center of focusing spot region irradiated by only the main pulse, and (3) the solid density plasma periphery region excited by the radiation and hot electrons emitted from the previous two regions. This creation of separate regions can occur due to the fast and ultra-intense interaction of the laser with the target. The fs pulse duration occurs so fast and its intensity so high that due to optical field ionization (Ammosov *et al.*, 1986) the atoms are ionized faster than they can radiate, which prevents radiation from intermittent ions. The spectrum from the stainless steel X-pinch

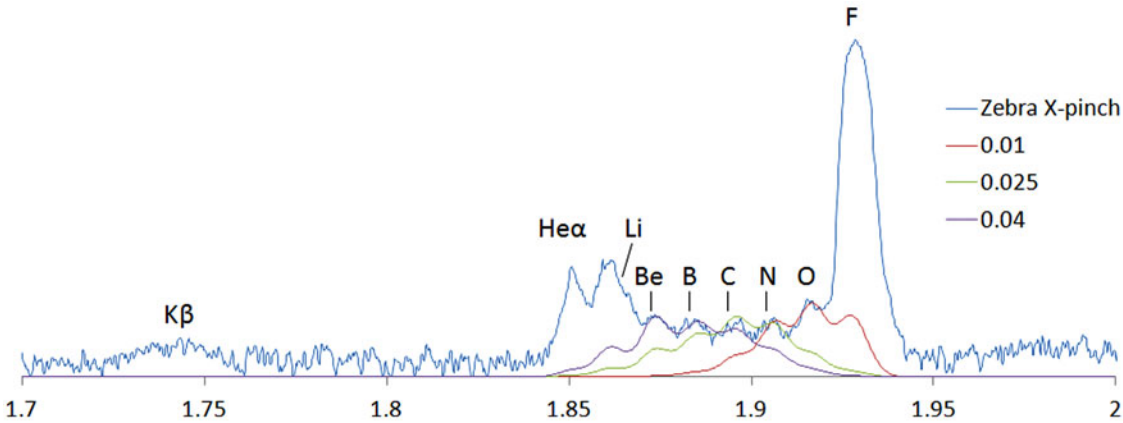

Fig. 4. Theoretical modeling showing the influence of different ionizations on the *K*-shell Fe experimental spectrum from a stainless steel X-pinch experiment performed on the Zebra generator at 1 MA. Modeling was done with $T_e = 170$ eV and $N_e = 1 \times 10^{20}$ cm^{-3} and three different hot electron concentrations (1, 2.5, and 4%). The experimental spectrum shows evidence of He-like to F-like ions.

https://doi.org/10.1017/S026303461600077X Published online by Cambridge University Press

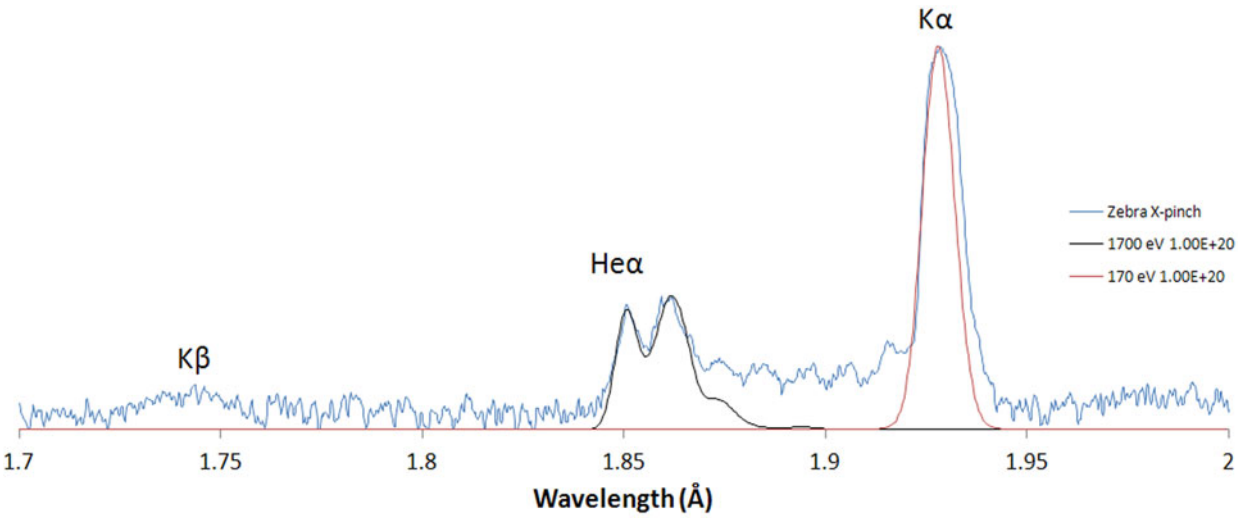

Fig. 5. Theoretical modeling for Stainless Steel X-pinch spectra estimating the plasma parameters of the highest T_e (1700 eV, 1×10^{20} cm^{-3}) and lowest T_e (170 eV, 1×10^{20} cm^{-3}) regions.

experiment was different because the intermediate ions were present. This is due to the much longer time scale of the experiment where the current typically rises for 30–60 ns prior to the first explosion of the X-pinch. The X-pinch spectrum had a strong Kα presence suggesting colder plasma surrounding the hotter core. This is similar to the Kα presence in the laser experiment; however the T_e for each experiment is significantly different (~10 eV laser and ~170 eV X-pinch). The colder laser-produced plasma is heated by X-ray radiation and fast electrons from the hotter regions while the colder plasma in the X-pinch experiment is also energized by the kinetic energy acquired while being accelerated by the explosions and implosions. This is seen in the different ionization levels of the transitions that dominate the Kα peaks. The hottest regions for each experiment are also quite different. The value of the electron densities differ by an order of magnitude (3×10^{21} cm^{-3} laser, 1×10^{20} cm^{-3} X-pinch) and the maximum values of the electron temperatures are quite different (3500 eV laser, 1700 eV X-pinch). The T_e difference is quickly noticeable by the presence of the Lyα in the laser-produced spectrum and not in the X-pinch spectrum.

Along with estimating the conditions of the laser-produced plasma, there was the hope to observe effects of X-ray pumping and hot electrons by analyzing KK and KL hollow ion emissions. The spectral regions where the KK and KL hollow ion transitions would be seen are at approximately 1.8–1.85 Å and 1.86–1.92 Å, respectively. Unfortunately the KK hollow ions spectral region has no evidence of spectral lines. The KL hollow ion spectral region includes multiple peaks of greater intensity that are also influenced by singly excited state transitions. The modeling of the laser-produced spectrum was improved with the inclusion of a small percentage of hot electrons for each of the three regions. The hot electrons were generated in the two hotter regions and dispersed to the coldest region to excite the near neutral atoms, which then produced the Kα emissions. The hot electrons also broadened the ionization distribution for the two hotter regions. Though the X-ray source intensity ~10^{17} W/cm^2 (Faenov *et al.*, 2015*a*) was enough to create KK hollow ions in aluminum, it was insufficient to create KK hollow ions with iron. The KL spectral region does have a reasonable presence though it is difficult to distinguish between the KL transitions and the singly excited state transitions. By considering the KK and KL emission regions it was determined that there were no sufficient effects from X-ray pumping on the spectra of hollow ions of iron in laser-produced plasma experimental conditions. At the same time it was shown that influence of hot electrons for formation of *K*-shell spectra of iron is rather large.

ACKNOWLEDGEMENTS

This work was partly supported by Russian Foundation for Basics Research (grant # 14-22-02089) and by RAS Presidium Program for basic research #11. This work was also supported by NNSA under DOE Cooperative Agreement DE-NA0001987 and grant DE-NA0003047.

REFERENCES

Abdallah, J., Batani, D., Desai, T., Lucchini, G., Faenov, A., Pikuz, T. & Magunov, A. (2007). High resolution X-ray emission spectra from picosecond laser irradiated Ge targets. *Laser Part. Beams* **25**, 245–252.

Ammosov, M.V., Delone, N.B. & Krainov, V.P. (1986). Tunnel ionization of complex atoms and of atomic ions in an alternating electromagnetic field. *Soviet Phys. J. Exp. Theoretical Phys.* **64**, 1191–1194.

Beiersdorfer, P. (2003). Laboratory X-ray astrophysics. *Ann. Rev. Astron. Astrophys.* **41**, 343–390.

https://doi.org/10.1017/S026303461600077X Published online by Cambridge University Press

Beiersdorfer, P., Phillips, T., Jacobs, V., Hill, K., Bitter, M., von Goeler, S. & Kahn, S.M. (1993). High-resolution measurements, line identification, and spectral modeling of Kα transitions in Fe XVIII–XXV. *Astrophys. J.* **409**, 846–859.

Beiersdorfer, P., von Goeler, S., Bitter, M. & Thorn, D.B. (2001). Measurement of the 3d→2p resonance to intercombination line-intensity ratio in neonlike Fe XVII, Ge XXIII, and Se XXV. *Phys. Rev. A* **64**, 032705.

Blasco, F., Stenz, C., Salin, F., Faenov, A.Ya., Magunov, A.I., Pikuz, T.A. & Skobelev, I.Yu. (2001). Portable, tunable, high-luminosity spherical crystal spectrometer with an x-ray charge coupled device, for high-resolution x-ray spectromicroscopy of clusters heated by femtosecond laser pulses. *Rev. Sci. Instrum.* **72**, 1956–1962.

Chen, S.N., Patel, P.K., Chung, H.K., Kemp, A.J., Le Pape, S., Maddox, B.R., Wilks, S.C., Stephens, R.B. & Beg, F.N. (2009). X-ray spectroscopy of buried layer foils irradiated at laser intensities in excess of 10^{20} W/cm^2. *Phys. Plasmas* **16**, 062701.

Colgan, J., Abdallah Jr., J., Faenov, A.Ya., Pikuz, S.A., Wagenaars, E., Booth, N., Culfa, O., Dance, R.J., Evans, R.G., Gray, R.J., Kaempfer, T., Lancaster, K.L., McKenna, P., Rossall, A.L., Skobelev, I.Yu., Schulze, K.S., Uschmann, I., Zhidkov, A.G. & Woolsey, N.C. (2013). Exotic dense-matter states pumped by a relativistic laser plasma in the radiation-dominated regime. *Phys. Rev. Lett.* **110**, 125001.

Colgan, J., Abdallah Jr., J., Faenov, A.Ya., Pikuz, T.A., Skobelev, I.Yu., Fortov, V.E., Fukuda, Y., Akahane, Y., Aoyama, M., Inoue, N. & Yamakawa, K. (2008). The role of hollow atoms in the spectra of an ultrashort-pulse-laser-driven Ar cluster target. *Laser Part. Beams* **26**, 83–93.

Colgan, J., Faenov, A.Ya., Pikuz, S.A., Tubman, E., Butler, N.M.H., Abdallah Jr., J., Dance, R.J., Pikuz, T.A., Skobelev, I.Yu., Alkhimova, M.A., Booth, N., Green, J., Gregory, C., Andreev, A., Lötz, R., Uschmann, I., Zhidkov, A., Kodama, R., McKenna, P. & Woolsey, N. (2016). Evidence of high-n hollow-ion emission from Si ions pumped by ultraintense x-rays from relativistic laser plasma. *Eur. Phys. Lett.* **114**, 35001.

Decaux, V., Beiersdorfer, P., Kahn, S.M. & Jacobs, V.L. (1997). High resolution measurement of the Kα spectrum of Fe XXV-XVIII: new spectral diagnostics of nonequilibrium astrophysical plasmas. *Astrophys. J.* **482**, 1076–1084.

Decaux, V., Beiersdorfer, P., Osterheld, A., Chen, M. & Kahn, S.M. (1995). High-resolution measurements of the Kα spectra of low-ionization species of iron: a new spectral signature of nonequilibrium ionization conditions in you supernova remnants. *Astrophys. J.* **443**, 464–468.

Drake, J.J., Swartz, D.A., Beiersdorfer, P., Brown, G.V. & Kahn, S.M. (1999). On photospheric fluorescence and the nature of the 17.62 Å feature in solar x-ray spectra. *Astrophys. J.* **521**, 839–843.

Eze, R.N.C. (2014). Fe Kα line in hard X-ray emitting symbiotic stars. *Monthly Notices R. Astron. Soc.* **437**, 857–861.

Faenov, A.Ya., Colgan, J., Hansen, S.B., Zhidkov, A., Pikuz, T.A., Nishiuchi, M., Pikuz, S.A., Skobelev, I.Yu., Abdallah, J., Sakaki, H., Sagisaka, A., Pirozhkov, A.S., Ogura, K., Fukuda, Y., Kanasaki, M., Hasegawa, N., Nishikino, M., Kando, M., Watanabe, Y., Kawachi, T., Masuda, S., Hosokai, T., Kodama, R. & Kondo, K. (2015*a*). Nonlinear increase of X-ray intensities from thin foils irradiated with a 200 TW femtosecond laser. *Sci. Rep.* **5**, 13436.

Faenov, A.Ya., Pikuz, S.A., Erko, A.I., Bryunetkin, B.A., Dyakin, V.M., Ivanenkov, G.V., Mingaleev, A.R., Pikuz, T.A., Romanova, V.M. & Shelkovenko, T.A. (1994). High-performance X-ray spectroscopic devices for plasma microsources investigations. *Phys. Scripta* **50**, 333–338.

Faenov, A.Ya., Skobelev, I.Yu., Pikuz, T.A., Pikuz Jr., S.A., Kodama, R. & Fortov, V.E. (2015*b*). Diagnostics of warm dense matter by high-resolution X-ray spectroscopy of hollow ions. *Laser Part. Beams* **33**, 27–39.

Gu, M.F. (2008). The flexible atomic code. *Can. J. Phys.* **86**, 675–689.

Hansen, S.B., Colgan, J., Faenov, A.Ya., Abdallah Jr., J., Pikuz Jr., S.A., Skobelev, I.Yu., Wagenaars, E., Booth, N., Culfa, O., Dance, R.J., Tallents, G.J., Evans, R.G., Gray, R.J., Kaempfer, T., Lancaster, K.L., McKenna, P., Rossall, A.K., Schulze, K.S., Uschmann, I., Zhidkov, A.G. & Woolsey, N.C. (2014). Detailed analysis of hollow ions spectra from dense matter pumped by X-ray emission of relativistic laser plasma. *Phys. Plasmas* **21**, 031213.

Kantsyrev, V.L., Rudakov, L.I., Safronova, A.S., Fedin, D.A., Ivanov, V.V., Velikovich, A.L., Esaulov, A.A., Chuvatin, A.S., Williamson, K., Ouart, N.D., Nalajala, V., Osborne, G., Shrestha, I., Yilmaz, M.F., Pokala, S., Laca, P.J. & Cowan, T.E. (2006). Planar wire array as powerful radiation source. *IEEE Trans. Plasma Sci.* **34**, 2295–2302.

Kiriyama, H., Mori, M., Nakai, Y., Shimomura, T., Sasao, H., Tanoue, M., Kanazawa, S., Wakai, D., Sasao, F., Okada, H., Daito, I., Suzuki, M., Kondo, S., Kondo, K., Sugiyama, A., Bolton, P.R., Yokoyama, A., Daido, H., Kawanishi, S., Kimura, T. & Tajima, T. (2010). High temporal and spatial quality petawatt-class Ti:sapphire chirped-pulse amplification laser system. *Opt. Lett.* **35**, 1497–1499.

Magunov, A.I., Faenov, A.Ya., Skobelev, I.Yu., Pikuz, T.A., Dobosz, S., Schmidt, M., Perdrix, M., Meynadier, P., Gobert, O., Normand, D., Stenz, C., Bagnoud, V., Blasco, F., Roche, J.R., Salin, F. & Sharkov, B.Yu. (2003). X-ray spectra of fast ions generated from clusters by ultrashort laser pulses. *Laser Part. Beams* **21**, 73–79.

Nishiuchi, M., Sakaki, H., Esirkepov, T.Zh., Nishio, K., Pikuz, T.A., Faenov, A.Ya., Skobelev, I.Yu., Orlandi, R., Sako, H., Pirozhkov, A.S., Matsukawa, K., Sagisaka, A., Ogura, K., Kanasaki, M., Kiriyama, H., Fukuda, Y., Koura, H., Kando, M., Yamauchi, T., Watanabe, Y., Bulanov, S.V., Kondo, K., Imai, K. & Nagamiya, S. (2015). Acceleration of highly charged GeV Fe ions from a low-Z substrate by intense femtosecond laser. *Phys. Plasmas* **22**, 033107.

Ouart, N.D., Safronova, A.S., Faenov, A.Ya., Pikuz, T.A., Gasilov, S.V., Calegari, F., Nisoli, M., De Silvestri, S., Stagira, S., Poletto, L. & Villoresi, P. (2011). Analysis of the simultaneous measurements of iron K- and L-shell radiation from ultrashort laser produced plasmas. *J. Phys. B: Atom. Mol. Opt. Phys.* **44**, 065602.

Phillips, K.J.H. (2012). The solar photospheric-to-coronal Fe abundance ratio from X-ray fluorescence lines. *Monthly Notices R. Astron. Soc.* **421**, 1757–1763.

Pikuz, S.A., Faenov, A.Ya., Colgan, J., Dance, R.J., Abdallah, J., Wagenaars, E., N. Booth, E., Culfa, O., Evans, R.G., Gray, R.J., Kaempfer, T., Lancaster, K.L., McKenna, P., Rossall, A.L., Skobelev, I.Yu., Schulze, K.S., Uschmann, I., Zhidkov, A.G. & Woolsey, N.C. (2013). Measurement and simulations of hollow atom X-ray spectra of solid-density relativistic plasma

https://doi.org/10.1017/S026303461600077X Published online by Cambridge University Press

created by high-contrast PW optical laser pulses. *High Energy Density Phys*. **9**, 560–567.

Ponti, G., Bianchi, S., Munoz-Darias, T., De Marco, B., Dwelly, T., Fender, R.P., Nandra, K., Rea, N., Mori, K., Haggard, D., Heinke, C.O., Degenaar, N., Aramaki, T., Clavel, M., Goldwurm, A., Hailey, C.J., Israel, G.L., Morris, M.R., Rushton, A. & Terrier, R. (2015). On the Fe K absorption – accretion state connection in the Galactic Centre neutron star X-ray binary AX J1745.6-2901. *Monthly Notices R. Astron. Soc*. **446**, 1536–1550.

Rajmal, J., Pradhan, A.K., Joshi, V., Shah, K.J., Trivedi, J.J., Kayasth, S.L., Shah, V.M. & Deshpande, M.R. (2006). The Fe-line feature in the x-ray spectrum of solar flares: first results from the SOXS mission. *Solar Phys*. **239**, 217–237.

Safronova, A.S., Kantsyrev, V.L., Esaulov, A.A., Ouart, N.D., Safronova, U.I., Shrestha, I. & Williamson, K.M. (2009). X-ray spectroscopy and imaging of stainless steel X-pinches with application to astrophysics. *Eur. Phys. J. Special Topics* **169**, 155–158.

Safronova, A.S., Kantsyrev, V.L., Esaulov, A.A., Ouart, N.D., Yilmaz, M.F., Williamson, K.M., Shrestha, I., Osborne, G.C., Greenly, J.B., Chandler, K.M., McBride, R.D., Chalenski, D.A., Hammer, D.A., Kusse, B.R. & LePell, P.D. (2008). Spectroscopy and implosion dynamics of low wire number nested arrays on the 1 MA COBRA generator. *Phys. Plasmas* **15**, 033302.

Zastrau, U., Audebert, P., Bernshtam, V., Brambrink, E., Kämpfer, T., Kroupp, E., Loetzsch, R., Maron, Y., Ralchenko, Yu., Reinholz, H., Röpke, G., Sengebusch, A., Stambulchik, E., Uschmann, I., Weingarten, L. & Förster, E. (2010). Temperature and Kα-yield radial distributions in laser-produced solid-density plasmas imaged with ultrahigh-resolution x-ray spectroscopy. *Phys. Rev. E* **81**, 026406.

https://doi.org/10.1017/S026303461600077X Published online by Cambridge University Press